Journal of Statistical Physics, Vol. 71, Nos. 3/4, 1993

From Ordered Bubbles to Random Stripes: Pattern Formation in a Hydrodynamic Lattice Gas

Daniel H. Rothman[1]

Received July 28, 1992; final November 10, 1992

A two-component momentum-conserving lattice gas with competing interactions is introduced in two dimensions. One interaction acts at short range and produces interfaces with surface tension. The second interaction, the negative of the first, acts at range a and produces modulated structures with approximate wavelength $2a$. Depending on particle density, species concentration, and relative interaction strength, the equilibrium patterns formed by the model range from isotropic mixed and unmixed phases to hexagonally-ordered bubbles to randomly-oriented stripes. A Ginzburg–Landau equation is proposed that qualitatively captures the basic features of these phase transitions.

KEY WORDS: Stripes; phase separation; lattice-gas automata; pattern formation.

1. INTRODUCTION

Many systems in nature, both in and out of equilibrium, exhibit spatially-modulated structures. Depending on the system, these periodic patterns can occur at widely varying scales. The "rolls" or "cells" one sees in Rayleigh–Bénard convection[1,2] are ubiquitous large-scale manifestations of such a periodic pattern. Other macroscopic examples are the structure of the visual cortex[3,4] and the patterns formed by ferromagnetic colloids subjected to an applied magnetic field.[5] At microscopic (i.e., subcontinuum) scales, modulated patterns occur in diverse systems, such as thin magnetic films,[6] Langmuir monolayers,[7,8] and diblock copolymers.[9]

Although the physics underlying each of these systems differ, one may consider the basic features of these modulated patterns to have resulted

[1] Department of Earth, Atmospheric, and Planetary Sciences, Massachusetts Institute of Technology, Cambridge, Massachusetts 02139.

0022-4715/93/0500-0641$07.00/0

from competing interactions. For example, in the case of convection, thermal buoyancy competes against viscous and thermal dissipation. Similarly, the two-dimensional labyrinthine patterns formed by ferrofluids are also the consequence of a competing interaction. In this case, a short-range attraction that manifests itself as surface tension competes against long-range dipolar magnetic repulsion.

In this paper, I introduce a simple, discrete, hydrodynamic model that contains just this generic feature of a competing interaction. The model, a momentum-conserving lattice-gas cellular automaton,[10] is a simple variant of the immiscible lattice gas (ILG)[11] in which the short-range ILG interaction that produces surface tension competes against an oppositely-signed ILG interaction that acts at long range. Because the interactions conserve momentum in addition to mass and particle type, the model retains much of the hydrodynamic properties of the simplest lattice gases.[12–15] Moreover, it allows one to consider how nonequilibrium dynamics affect the growth of modulated patterns. This paper, however, discusses only the equilibrium properties of the model. The various phase transitions from one type of pattern to another are first illustrated by numerical simulation. A simple Ginzburg–Landau equation is then proposed that reveals qualitatively the main features of these transitions.

2. THE COMPETING-INTERACTION LATTICE GAS

The competing-interaction lattice gas is a variant of the immiscible lattice-gas (ILG) model,[11] which is in turn a two-component extension of the simplest hydrodynamic lattice gas, due to Frisch, Hasslacher, and Pomeau (FHP).[10] In the FHP model, identical particles of unit mass move with unit speed from site to site on a triangular lattice. When particles meet at a site, they obey simple collision rules that conserve mass and momentum. The macroscopic behavior of this lattice gas has been shown to be very close to the incompressible Navier–Stokes equations.[12–15]

In the immiscible lattice gas, each site on the two-dimensional triangular lattice may contain red particles, blue particles, or both, but at most one particle (red or blue) may move in each of the six directions $\mathbf{c}_1,\ldots,\mathbf{c}_6$. Each site may also have a seventh stationary, or rest, particle moving with velocity $\mathbf{c}_0$ and subject to the same exclusion rule. The configuration at a site $\mathbf{x}$ is then described by the Boolean variables $r=\{r_i\}$ and $b=\{b_i\}$, which indicate the presence (1) or absence (0) of a red or blue particle, respectively, moving with velocity $\mathbf{c}_i$. Note that the exclusion rule prevents r_i and b_i from both being equal to one.

The most important feature of the ILG is the existence of a phase-separation transition and surface tension, both of which result from the

following dynamics. At a site $\mathbf{x}$ undergoing a collision, a color flux $\mathbf{q}$ is defined to be the difference between the red momentum and the blue momentum:

$$\mathbf{q}[r(\mathbf{x}), b(\mathbf{x})] \equiv \sum_{i=1}^{6} \mathbf{c}_i [r_i(\mathbf{x}) - b_i(\mathbf{x})] \tag{1}$$

The local color gradient,

$$\mathbf{f}(\mathbf{x}) \equiv \sum_i \mathbf{c}_i \sum_j [r_j(\mathbf{x}+\mathbf{c}_i) - b_j(\mathbf{x}+\mathbf{c}_i)] \tag{2}$$

is also computed. The ILG collision rule is antidiffusive: it maximizes the flux of color in the direction of the local color gradient. The result of a collision, $r \to r'$, $b \to b'$, is the configuration that maximizes

$$\mathbf{q}(r', b') \cdot \mathbf{f} \tag{3}$$

such that the number of red particles and the number of blue particles is conserved,

$$\sum_i r_i' = \sum_i r_i, \qquad \sum_i b_i' = \sum_i b_i \tag{4}$$

and so is the total momentum:

$$\sum_i \mathbf{c}_i (r_i' + b_i') = \sum_i \mathbf{c}_i (r_i + b_i) \tag{5}$$

A competing interaction is included in the model by simply incorporating within the collision rule an additional dependence on a *coarse-grained* gradient, but with opposite sign. Specifically, the gradient

$$\mathbf{g}_a(\mathbf{x}) \equiv \sum_i \mathbf{c}_i \sum_j [r_j(\mathbf{x}+a\mathbf{c}_i) - b_j(\mathbf{x}+a\mathbf{c}_i)] \tag{6}$$

is computed, where the parameter a defines the scale of coarse-graining.[2] The result of a collision, $r \to r'$, $b \to b'$, is then determined by the r' and b' that maximize

$$\mathbf{q}(r', b') \cdot \left(\frac{\mathbf{f}}{|\mathbf{f}|} - \alpha \frac{\mathbf{g}_a}{|\mathbf{g}_a|} \right) \tag{7}$$

[2] To increase isotropy, the implementation used here actually uses 12 instead of 6 points to estimate $\mathbf{g}_a$, but the difference is negligible.

where $\alpha \geqslant 0$ is a parameter that controls the relative strength of the long-range interaction, and mass, momentum, and color are locally conserved as before. This particular form of a competing interaction is motivated only by simplicity, not by a particular physical system.

3. RESULTS FROM SIMULATIONS

Simulations of the competing interaction model show an interesting dependence not only on α, but also on the concentration θ of the red phase. Below I describe results obtained when the reduced density $d = 0.5$ (i.e., the average occupancy of a site is half the maximum occupancy). This density is always above the θ-dependent critical density needed for the ILG to undergo phase separation.[16] In each example the lattice contains 128×128 points, the boundaries are periodic, the long-range interaction length $a = 5$, and the initial state is a random mixture of red and blue particles.

Figure 1 shows two snapshots of configurations of the competing-interaction model, 1000 time steps apart, for the case $\alpha = 1.0$ and $\theta = 0.5$. These randomly-oriented stripes quickly form after about 100 time steps, after which the model appears to settle in an equilibrium state characterized by large and frequent fluctuations of the pattern, the effect of which is evident from the changes to the pattern over the 1000-time-step duration illustrated here. Computations of power spectra of these two-dimensional patterns show that the average stripe width is 3.6 lattice units, or $0.72a$, and that the pattern is statistically isotropic within experimental accuracy.

Figure 2 shows a result with parameters identical to those used in Fig. 1, but with $\alpha = \infty$; i.e., no short-range attraction. This result shows

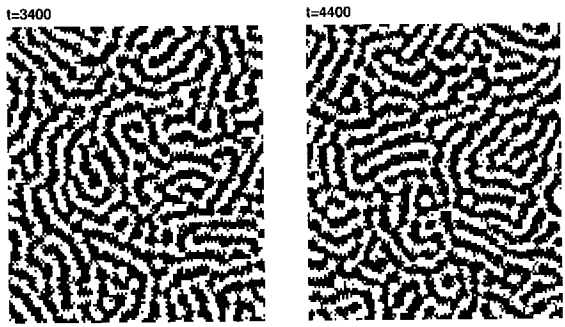

Fig. 1. Results from a simulation of the competing-interaction lattice gas. The long-range interaction strength is $\alpha = 1.0$ and the red (black) concentration is $\theta = 0.5$. The initial configuration at time $t = 0$ was a random mixture. The difference between the two snapshots is due to fluctuations of the pattern.

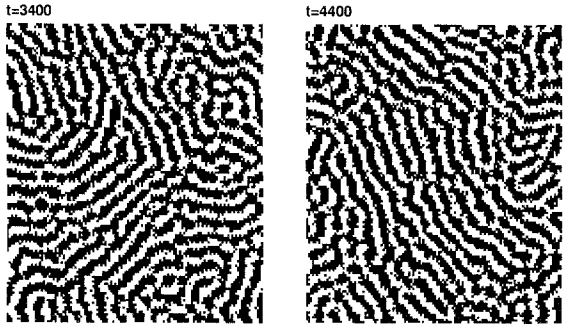

Fig. 2. Simulation of the competing-interaction lattice gas, with $\alpha = \infty$ and $\theta = 0.5$. Comparison with the case $\alpha = 1.0$ in Fig. 1 shows how increasing α increases the correlation length of the stripe orientations.

that the correlation length of stripe orientations increases weakly with increasing α, a consequence of the diminishing influence of the tendency of the short-range interaction to minimize total surface length.

Figure 3 illustrates the dependence of the model on the red concentration θ, where here $\theta = 0.33$ and $\alpha = 1.0$. One sees hexagonally-ordered bubbles, separated by a distance of order a. Initially the hexagonal ordering is only local, but after time the ordering extends through the entire system. The final ordering of the bubbles does not correspond to any lattice direction, but it may possibly result from either the periodic boundaries or the specific scheme used to compute $\mathbf{g}_a$.

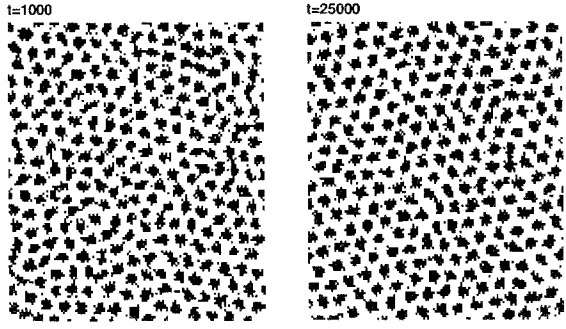

Fig. 3. Simulation of the competing-interaction lattice gas, with $\alpha = 1.0$ and $\theta = 0.33$. Comparison with the case $\theta = 0.5$ in Fig. 1 shows that significantly off-critical concentrations can result in hexagonally-ordered bubbles, while critical concentrations result in stripes. The initial, mostly local, hexagonal ordering is unstable, while the later, global, hexagonal ordering persists for long times.

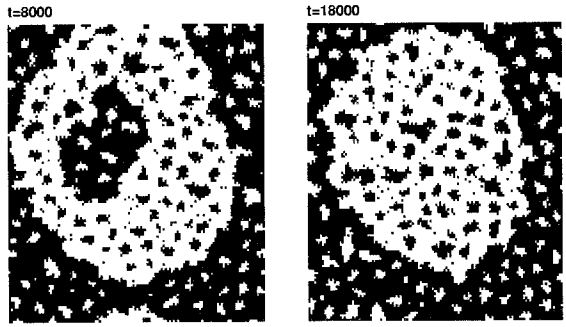

Fig. 4. Simulation of the competing-interaction lattice gas, with $\alpha = \alpha_c = 0.26$ and $\theta = 0.5$. As in Figs. 1–3, the initial configuration was a random mixture. If α were chosen less than α_c, the result would be a simple phase separation; $\alpha > \alpha_c$ would result in a pattern like those in Figs. 1 and 2. Here, one sees both a two-phase coexistence (i.e., black separates from white), but also hexagonally-ordered bubbles within each phase.

Figure 4 shows a surprising result obtained for $\alpha = \alpha_c = 0.26$, where α_c is the critical value of α above which the model creates stripes as in Figs. 1 and 2, and below which the model results in the simple phase separation described in refs. 11 and 16. Here the concentration $\theta = 0.5$, so the only difference with Figs. 1 and 2 is the value of α. The result, a coexistence of both the bubble phase and the phase-separated state, probably occurs because α is low enough to prevent the formation of stripes, but still high enough to create bubbles from the minority of red particles that would normally be dissolved in the blue phase, and likewise from the blue particles dissolved in the red phase. The pattern is qualitatively similar to those seen in ref. 8.

4. GINZBURG–LANDAU EQUATION

To understand why specific patterns are selected, one normally would compare the free energies of the various patterns. However, since the ILG and its variants are not thermal models, no straightforward analog of a free energy exists.[16,17] Numerical simulations of the ILG show, however, (1) the existence of a curve analogous to a classical spinodal curve[16]; and (2) the apparent minimization of some quantity (e.g., total surface length) during nonequilibrium evolution from a mixed to an unmixed state. Thus I postulate that a nondimensional function

$$V[\phi(\mathbf{x})] = \int_{-\infty}^{\infty} \int_{-\infty}^{\infty} F[\phi(\mathbf{x})]\, d\mathbf{x} \tag{8}$$

is minimized by ILG models, where, in analogy with the classical Landau expansion,[18]

$$F[\phi(\mathbf{x})] = b_2\phi^2(\mathbf{x}) + b_4\phi^4(\mathbf{x}) + \cdots \tag{9}$$

and ϕ is the deviation of the red concentration from 0.5. Above the critical density (i.e., below the critical "temperature"), $b_2 < 0$ and $b_4 > 0$, yielding two symmetric minima representative of the blue-rich phase and the red-rich phase. In the following, V will be referred to as a free energy, but this term is used here only in analogy with real systems.

To take account of the competing interactions in the new lattice-gas model, two space-dependent terms are added to Eq. (9). One is representative of the usual ILG interaction, and is proportional to $(\nabla\phi)^2$. The other, due to the long-range repulsive interaction, is proportional to $(\nabla\langle\phi\rangle_a)^2 = \langle\nabla\phi\rangle_a^2$, where

$$\langle f(x_1, x_2)\rangle_a = \frac{4}{\pi a^2}\int_{-\infty}^{\infty}\int_{-\infty}^{\infty} \Pi\left(\frac{(u^2+v^2)^{1/2}}{a}\right) f(x_1-u, x_2-v)\, du\, dv \tag{10}$$

and Π is the tophat defined by[3]

$$\Pi(r) = \begin{cases} 1, & |r| \leqslant 1/2 \\ 0, & |r| > 1/2 \end{cases} \tag{11}$$

These space-dependent terms are then added to Eq. (9) to obtain the following Ginzburg–Landau equation:

$$F(\phi) = b_2\phi^2 + b_4\phi^4 + a^2[(\nabla\phi)^2 - \alpha\langle\nabla\phi\rangle_a^2] \tag{12}$$

The parameter $\alpha \geqslant 0$ controls the relative strength of the long-range interaction and the factor of a^2 is chosen for dimensional consistency (after an appropriate rescaling of b_2 and b_4). Equation (12) is similar to the Ginzburg–Landau equations studied in refs. 6 and 7 except for the construction of the repulsive interaction term, which is motivated here by the two-scale symmetry in Eq. (7).

The gradient terms in Eq. (12) have the following interpretation. The positive contribution represents ILG surface tension, which acts to minimize surface lengths. The negative contribution derives from the long-range repulsive interaction of the competing-interaction model; this term acts to *maximize* total surface length, but at a coarse-grained length scale. The

[3] The diameter of the convolutional smoother is chosen to be a times unity, where unity is the diameter of the (identity) operator that may be considered to have been applied to the unsmoothed concentration field.

competition between these two contributions can result in the selection of a dominant wavenumber of concentration variations. By decomposing ϕ via the Fourier transform relation

$$\hat{\phi}(\mathbf{k}) = \int_{-\infty}^{\infty} \int_{-\infty}^{\infty} \phi(\mathbf{x})\, e^{-i\mathbf{k}\cdot\mathbf{x}}\, d\mathbf{x} \tag{13}$$

we find, assuming $\hat{\phi}(\mathbf{k}) = \hat{\phi}_0$, that the dominant wavenumber $k = |\mathbf{k}|$ is determined by the particular k that least contributes to the free energy V, or, equivalently, to the integral

$$\int_0^{\infty} [k^2 - (16\alpha/a^2)\, J_1^2(ak/2)]\, k\hat{\phi}^2(k)\, dk \tag{14}$$

Here J_1 is a Bessel function of the first kind, order 1. For reasonable choices of α and a, the term in brackets on the right-hand side is minimized close to the absolute minimum of $-J_1^2(ak/2)$, or for $ak \approx 0.58$. Thus the competing interactions predict a modulated structure with wavenumber $q/2\pi \approx 0.58/a$. This is about 10–20% short of values observed in the lattice-gas model.

In a manner similar to refs. 6, 7, and 19, we consider two trial functions for $\phi(\mathbf{x})$, a striped phase

$$\phi_S = \phi_0 + \phi_q \cos qx \tag{15}$$

and a hexagonal phase

$$\phi_H = \phi_0 + \sum_{i=1}^{3} \phi_q \cos(\mathbf{q}_i \cdot \mathbf{x}) \tag{16}$$

where in the latter case,

$$|\mathbf{q}_i| = q, \qquad \sum_{i=1}^{3} \mathbf{q}_i = 0 \tag{17}$$

Although the parallel stripes implied by ϕ_S are clearly not the random stripes of Fig. 1, for the purpose of constructing a phase diagram this approximation is adequate.

Substitution of these trial solutions into Eqs. (12) and (8) gives, for the striped phase,

$$V_S = b_2\left(\phi_0^2 + \frac{\phi_q^2}{2}\right) + b_4\left(\phi_0^4 + 3\phi_0^2\phi_q^2 + \frac{3}{8}\phi_q^4\right) + \frac{1}{2}\phi_q^2 a^2 q^2 - 16\alpha\phi_q^2 J_1^2\left(\frac{aq}{2}\right) \tag{18}$$

and for the hexagonal phase,

$$V_H = b_2\left(\phi_0^2 + \frac{3}{2}\phi_q^2\right) + b_4\left(\phi_0^4 + 9\phi_0^2\phi_q^2 + \frac{45}{8}\phi_q^4\right) + \frac{3}{2}\phi_q^2 a^2 q^2 - 48\alpha\phi_q^2 J_1^2\left(\frac{aq}{2}\right) \tag{19}$$

After defining the dimensionless parameters

$$c_0^2 = \frac{b_4\phi_0^2}{a^2q^2}, \qquad c_q^2 = \frac{b_4\phi_q^2}{a^2q^2}, \qquad \delta = \frac{b_2\phi_q^2}{a^2q^2} \tag{20}$$

Eqs. (18) and (19) simplify to

$$V_S = \delta\left(c_0^2 + \frac{c_q^2}{2}\right) + \left(c_0^4 + 3c_0^2c_q^2 + \frac{3}{8}c_q^4\right) + \frac{1}{2}c_q^2 - \frac{16\alpha}{a^2q^2}c_q^2 J_1^2\left(\frac{aq}{2}\right) \tag{21}$$

and

$$V_H = \delta\left(c_0^2 + \frac{3}{2}c_q^2\right) + \left(c_0^4 + 9c_0^2c_q^2 + \frac{45}{8}c_q^4 + 6c_0c_q^3\right) + \frac{3}{2}c_q^2 - \frac{48\alpha}{a^2q^2}c_q^2 J_1^2\left(\frac{aq}{2}\right) \tag{22}$$

where for clarity the terms are organized as they appear in Eq. (12).

The value of the modulation amplitude c_q pertinent to each phase is obtained by minimizing V_S and V_H with respect to c_q. If c_q is set to zero, then we obtain the free energy of the isotropic, unmodulated phase,

$$V_I = \delta c_0^2 + c_0^4 \tag{23}$$

As in refs. 6 and 7, a phase diagram in the plane of dimensionless "temperature" δ and concentration c_0 is obtained by minimizing $V_i - \mu c_0$ with respect to i, where i may be S, H, or I, and μ is the "chemical potential." The usual common tangent construction then yields not only regions where pure hexagonal, striped, or isotropic phases exist, but also regions where two phases can coexist. After performing these minimizations numerically, we obtain the phase diagram in Fig. 5. In this case, $\alpha = 2.0$. The results in the vicinity of $c_0 = 0$ and $\delta \approx 0$ show features qualitatively similar to what was evident in simulations of the lattice-gas model: quenched mixtures with nearly equal fractions of blue and red result in stripes, while the hexagonally-ordered bubble phase occurs when the

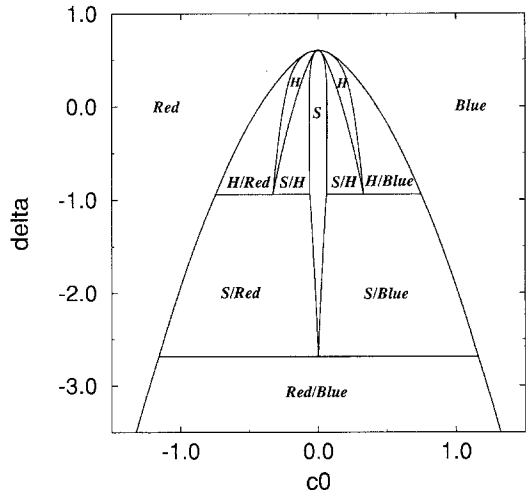

Fig. 5. The phase diagram that results from an analysis of Eq. (12), for the case $\alpha = 2.0$. Here δ is a dimensionless temperature and c_0 is proportional to concentration minus one-half. Isotropic phases are either red or blue, the striped phase is denoted by S, and the hexagonal phase by H. The S/H, H/Red, etc., denote a two-phase coexistence. The phase diagram is only valid in the region near the critical point $c_0 = 0$, $\delta \approx 0$. For $\alpha > \alpha_c = 1.25$ the phase diagram remains qualitatively the same; for $\alpha < \alpha_c$, however, the striped and hexagonal phases disappear, leaving only isotropic one-phase and two-phase regions.

minority concentration is significantly less than 50%. In Fig. 5 the hexagonal phase disappears below $\delta \approx -1$, while the stripe phase disappears below $\delta \approx -2.7$. This behavior is not present in the lattice-gas model, but it occurs here because these regions are far from the critical point and therefore far from the region of validity of Eq. (12).

Another interesting point concerns the dependence of the phase diagram on α, the strength of the long-range repulsive interaction. For $\alpha > \alpha_c = 1.25$, the phase diagram remains essentially as in Fig. 5, but with particular boundaries in different locations. (For example, the critical temperature δ_c at $c_0 = 0$ increases with increasing α.) However, when $\alpha < \alpha_c$, the modulated stripe and hexagonal phases disappear from the phase diagram, leaving only isotropic two-phase and one-phase regions. Although the lattice-gas result in Fig. 4 occurs at the analogous critical point in the lattice-gas model (for which $\alpha_c = 0.26$), Eq. (12) is too simple to capture that behavior. (In the analytic formulation, the pattern in Fig. 4 would correspond to simultaneous coexistence of red-rich and blue-rich hexagonal and isotropic phases.)

Lastly, it is interesting to note that the Ginzburg–Landau phase diagram for $\alpha > \alpha_c$ is qualitatively similar to the one obtained in ref. 7 in a

study of Langmuir monolayers, in which the long-range repulsive interaction was integrated across the entire two-dimensional plane. Although Eq. (12) is comparatively a mathematical artifice, its simple two-scale interaction is sufficient to capture a similar equilibrium phase diagram.

4. CONCLUSIONS

The competing-interaction lattice-gas model yields a variety of interesting two-dimensional modulated patterns. The randomly-striped and hexagonally-ordered patterns have been observed in other models,[20–22] but the model presented here is in a sense simpler, in that the competition arises from a simple two-scale interaction of identical terms, differing only by their sign and scale.

The Ginzburg–Landau equation studied here is a qualitative analytical model of the phase transitions observed in the competing-interaction lattice-gas. As in the lattice gas, a phase transition from the striped phase to the hexagonal phase occurs at off-critical concentrations. Although the long-range interaction term of this new Ginzburg–Landau equation is considerably different than the one studied in ref. 7, essentially the same phase diagram is derived. This may be viewed as a consequence of the wavenumber selection implied by the convolutional smoother in Eq. (10). This convolutional operator is perhaps the simplest operator that creates wavenumber selection.[3,4]

A surprising result of the competing-interaction lattice-gas model is its behavior in the vicinity of the critical value of α, the strength of the long-range interaction. In this case one can see bubbles within bubbles, an interesting coexistence of different phases that is not predicted by the Ginzburg–Landau analysis.

Finally, I note that this study has explored only the equilibrium properties of the competing-interaction lattice gas. Since the model includes hydrodynamics, its nonequilibrium pattern formation, including the effects of shear flow,[23] are of considerable interest for future work.

ACKNOWLEDGMENTS

This work was supported in part by the sponsors of the MIT Porous Flow Project and NSF Grant 9017062-EAR. The project was initiated during a visit to the University of Chicago, where support was obtained from the Department of Geophysical Sciences, the James Franck Institute, and the Computational and Applied Mathematics Program. I thank A. Karma, E. Presutti, T. Witten, W. Young, and S. Zaleski for interesting discussions.

REFERENCES

1. J. Swift and P. Hohenberg, *Phys. Rev. A* **15**:319 (1977).
2. P. Manneville, *Dissipative Structures and Weak Turbulence* (Academic Press, San Diego, 1990).
3. N. V. Swindale, *Proc. R. Soc. Lond. B* **215**:211 (1982).
4. E. Bienenstock, in *Synergetics of the Brain*, E. Basai, H. Flohr, H. Haken, and A. Mandell, eds. (Springer-Verlag, Berlin, 1983), pp. 250–263.
5. R. Rosensweig, *Ferrohydrodynamics* (Cambridge University Press, Cambridge, 1985).
6. T. Garel and S. Doniach, *Phys. Rev. B* **26**:325 (1982).
7. D. Andelman, F. Brochard, and J.-F. Joanny, *J. Chem. Phys.* **86**:3673 (1987).
8. M. Seul and M. J. Sammon, *Phys. Rev. Lett.* **64**:1903 (1990).
9. F. S. Bates, *Science* **251**:898 (1991).
10. U. Frisch, B. Hasslacher, and Y. Pomeau, *Phys. Rev. Lett.* **56**:1505 (1986).
11. D. H. Rothman and J. M. Keller, *J. Stat. Phys.* **52**:1119 (1988).
12. U. Frisch, D. d'Humières, B. Hasslacher, P. Lallemand, Y. Pomeau, and J.-P. Rivet, *Complex Systems* **1**:648 (1987).
13. L. Kadanoff, G. McNamara, and G. Zanetti, *Phys. Rev. A* **40**:4527 (1989).
14. G. Zanetti, *Phys. Rev. A* **40**:1539 (1989).
15. S. Wolfram, *J. Stat. Phys.* **45**:471 (1986).
16. D. H. Rothman and S. Zaleski, *J. Phys.* (Paris) **50**:2161 (1989).
17. F. J. Alexander, I. Edrei, P. L. Garrido, and J. L. Lebowitz, Phase transitions in a probabilistic cellular automaton: Growth kinetics and critical properties, preprint.
18. L. D. Landau and E. M. Lifshitz, *Statistical Physics* (Pergamon Press, New York, 1980).
19. S. A. Brazovskii, *Zh. Eksp. Teor. Fiz.* **68**:175 (1975) [*Sov. Phys. JETP* **41**:85 (1975)].
20. Y. Oono and Y. Shiwa, *Mod. Phys. Lett. B* **1**:49 (1987).
21. C. Roland and R. Desai, *Phys. Rev. B* **42**:6658 (1990).
22. M. M. Hurley and S. J. Singer, Domain energies of the dipolar lattice gas, preprint.
23. A. Onuki, *J. Chem. Phys.* **87**:3692 (1987).